

Chapter 4

The Short Baseline Near Detector and The Booster Neutrino Beam

Chapter 4 Opening

4.1 The Short-Baseline Near Detector Physics Program

The Short-Baseline Near Detector (SBND) is part of the Short-Baseline Neutrino (SBN) Program located at Fermilab [1]. The program consists of three LArTPC detectors: SBND, MicroBooNE, and Imaging Cosmic Rare Underground Signals (ICARUS), positioned at distances of 110 m, 470 m, and 600 m, respectively, on axis to the target of the Booster Neutrino Beam (BNB) as shown in Fig. 4.1. The near-far detector setup was designed to search for the potential existence of sterile neutrinos with an eV mass scale, driven by a series of anomalies observed by previous short baseline experiments.

The Liquid Scintillator Neutrino Detector (LSND) experiment utilised a stopped pion source to probe $\bar{\nu}_e$ via inverse beta decay and reported an excess of signal to background at low energies with a 3.8σ level [2]. Meanwhile, the MiniBooNE experiment was a neutrino accelerator experiment to measure the entire phase space covered by the LSND result [3]. The detector observed an excess of ν_e ($\bar{\nu}_e$) in ν_μ ($\bar{\nu}_\mu$) beam mode showing a discrepancy from the SM with a significance level of 4.5σ (2.8σ), reaching 6.0σ when combined with the LSND data. Additionally, results from the nuclear reactors experiments indicated a deficit of $\bar{\nu}_e$ fluxes to expectations at a 3σ level [4, 5], as well contained spectral features consistent with a fourth neutrino addition [6, 7]. Furthermore, gallium solar neutrino experiments observed an overall deficit in ν_e fluxes at a 3σ level during calibrations using radioactive neutrino sources [8, 9]. These four main anomalous results collectively suggest the mixing of SM neutrinos with a fourth non-weakly-interacting neutrino at a short baseline to energy ratio of $L/E \approx 1$ m/MeV, a phenomenon known as sterile neutrino oscillation [1]. The goal of the SBN program is to pioneer the search for eV-scale sterile neutrino oscillations, covering the parameter phase space previously allowed by past experiments at a significance level of $\geq 5\sigma$.

Additionally, measurements of neutrino-nucleus interactions plays a crucial role in the physics program of SBND, serving as a critical element in understanding neutrino oscillation [10]. Being the nearest to the beam, SBND is presented with a unique opportunity to observe the largest unoscillated neutrino fluxes among the three detectors. Over the 3-year operational span, SBND aims to record a staggering 10 million neutrino events, originating from 10×10^{20} Proton-On-Target (POT) interactions [1]. This will establish SBND as the world leader in statistics for neutrino-argon cross section measurements. More than 6 millions ν_μ charged current (CC) events will be collected, reducing the statistics uncertainty well below the percent. Moreover, SBND is expected to record 45,000 ν_e CC events, marking the most extensive statistics for both inclusive and exclusive measurements of this channel to date. These measurements will be extremely beneficial for advancing the objectives of the

4.1 The Short-Baseline Near Detector Physics Program

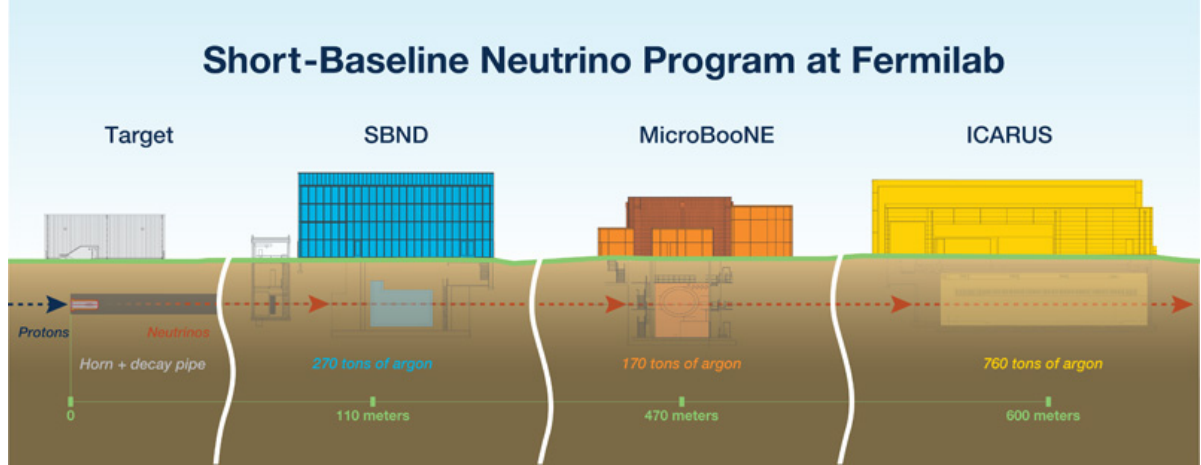


Fig. 4.1 Graphic showing the three LArTPC detectors made up the Short-Baseline Neutrino program: SBND, MicroBooNE and ICARUS. Their respective masses and distances with respect to the target of the Booster Neutrino Beam are shown. Fig. from [1].

SBN physics program, as well as contributing to the physics goals of the Deep Underground Neutrino Experiment (DUNE), which employs argon as its target material.

Finally, a key aspect of the physics program of the SBND experiment is the exploration of new scenarios leading to BSM physics. Close proximity to a high-intensity beam and the resulting large statistics enable searches for very weakly coupled interactions coming from the BNB [1]. Namely, heavy neutral leptons, the primary focus of this thesis, can be produced by the BNB and subsequently decay in-flight into SM observables for detection [11]. Another compelling BSM candidate is light dark matter, which can be produced from neutral meson decay or proton bremsstrahlung in the BNB [12]. Postulated by thermal relic models, these light dark matter particles could reach sub-GeV-scale masses. The particles may scatter and decay, resulting in electromagnetic showers without any hadronic activities inside the detector. Moreover, the dynamic mass mechanism of neutrinos opens avenues for new physics in the dark sector. The dark neutrino model proposes that right-handed neutrinos can scatter with nuclei to produce dark gauge bosons, subsequently decaying into di-lepton pairs [13]. In the case where the leptons are electrons, this could potentially explain the low energy excess anomalies observed by LSND and MiniBooNE [14]. These represent just a few examples of the diverse array of BSM scenarios that can be explored at the SBND detector. Other unmentioned possibilities such as new interactions, extra dimensions, violations of Lorentz and CPT symmetries, among others, contribute to the rich physics program of SBND [1].

4.2 The Booster Neutrino Beam

The SBND detector directly measures the neutrino flux coming from the BNB. A comprehensive technical details of the BNB can be found in Ref. [15]. The BNB operates by extracting protons with a kinetic energy of 8 GeV from the Booster synchrotron in spills made up of 7 to 11 pulses in a row at a frequency of 15 Hz, averaging to a rate of ~ 5 Hz. Each spill delivers 5×10^{12} protons within a beam spill window lasting $1.6 \mu\text{s}$. The structure of a beam spill structure consists of 81 individual neutrino bucket, with a Gaussian width of 1.308 ns and a spacing of 19 ns [16]. This distinctive bucket structure can be resolved with sufficient timing resolution, enabling cosmics rejection and BSM physics searches occurring outside of the bucket. Fig. 4.2 illustrates such capability of the Cosmic Ray Tagger (CRT) system at SBND, which collected data from the BNB from 2017 to 2018 [17].

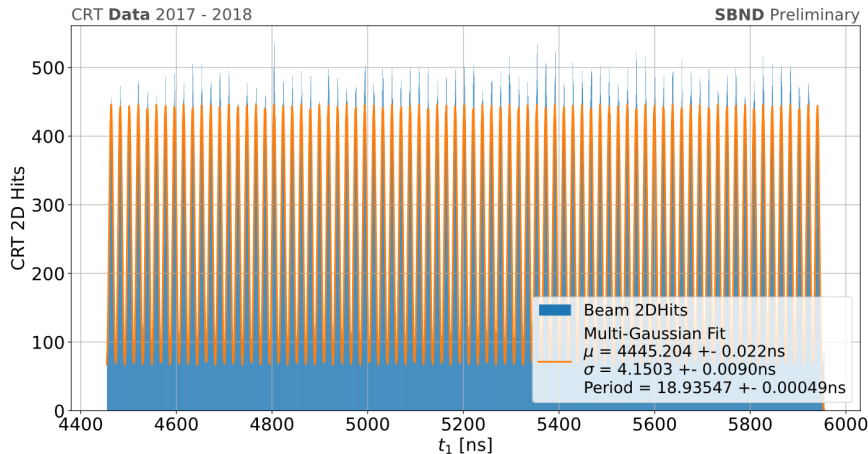


Fig. 4.2 The BNB beam structure was measured and resolved using the CRT system of SBND as a beam telescope during a run from 2017 - 2018. The beam structure can be seen, made up of 81 neutrino buckets. Fig. from [17].

The neutrino production process in the BNB is illustrated in Fig. 4.3. Initially, protons are injected into the Booster synchrotron and accelerated from 400 MeV to 8 GeV kinetic energy. Their intensity is measured by two steroids, while their positioning and timing are monitored by beam position monitors and Resistive Wall Monitor (RWM) [18]. Upon exiting the Booster, the proton beam traverses focusing and defocusing quadrupole and dipole magnets before being steered and focused onto the target of the BNB. The target consists of a beryllium cylinder measuring 71.1 cm in length and 0.51 cm in radius. The choice of beryllium was motivated by its replaceable ability in the event of radioactivity issues, as well as its ability to facilitate sufficient energy loss via an air cooling system. The target is placed inside a pulsed horn system, which acts as a 170 kA electromagnet to focus the secondary

4.2 The Booster Neutrino Beam

mesons resulting from protons colliding on the target. The polarity of the horn can be adjusted to focus positive (negative) mesons for operation in neutrino (antineutrino) mode. Downstream of the horn assembly, a concrete collimator of dimensions 214 cm in length and 30 cm in radius (expanding to 35.5 cm from upstream to downstream end) absorbs particles that do not contribute to the neutrino flux, thereby reducing radiation elsewhere in the beamline. The focused particles then propagate through an air-filled cylindrical decay region spanning 45 m, terminated by a steel and concrete absorber located 50 m from the upstream face of the target. Secondary mesons decay into tertiary neutrinos within this region, while long-lived muons are absorbed by the absorber. Subsequently, the neutrinos traverse through a dirt region before reaching the SBND detector.

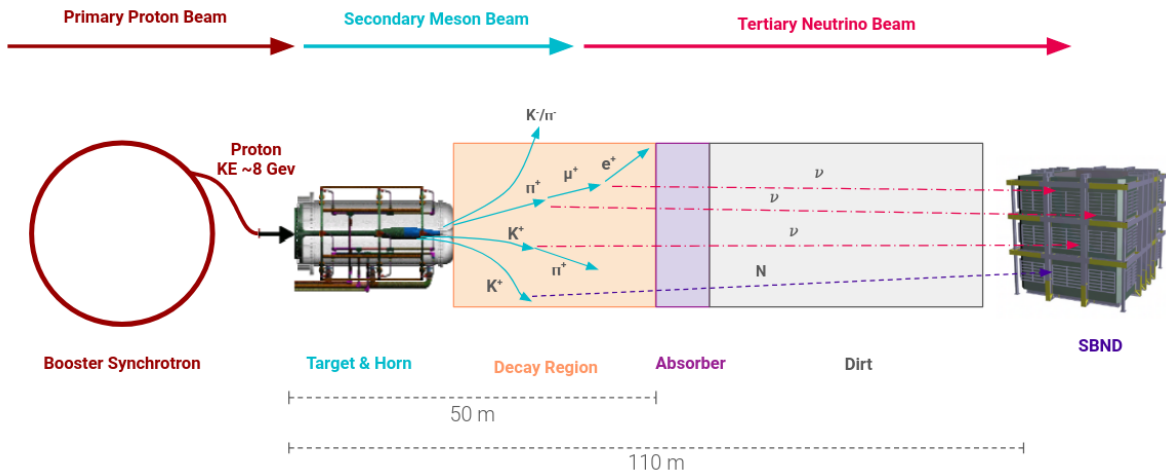


Fig. 4.3 Diagram of the neutrino production in the BNB. Primary proton beam (brown arrow) is collided onto the target to produce secondary mesons (blue arrows), which subsequently decay into tertiary neutrinos (pink arrows). The production mode for heavy neutral leptons from kaon decays is also shown (purple arrow).

The beam is simulated using GEANT4 with different tunings for the composition of the secondary mesons and hadrons produced from $p + Be$ interactions [15]. The π^\pm production is tuned to the HARP data set using Sanford-Wang parametrisation . The K^+ production is extrapolated to the global K^+ production data using Feynman scaling-based parametrisation, and further constrained by SciBooNE's direct measurements of K^+ production from the BNB [19]. Other secondary hadrons and mesons such as p , n and K^- are modelled using the MARS hadronic interactions, however their overall contribution to the neutrino flux is small. Interaction cross sections of $p/n + Be$ and $\pi^\pm + Be$ are also incorporated in flux

predictions [20]. The systematics uncertainties associated the BNB flux are calculated by a re-weighting process, which will be presented in Chapter ??.

Fig. 4.4 depicts the primary contributors to the secondary meson fluxes at the BNB, namely pions and kaons. A small fraction of muons resulting from pion decays also contribute to the fluxes. These fluxes are shown for the BNB operating in neutrino mode, mainly composed of positively charged mesons. As discussed in Sec. 2.2, the flux of HNL comes from K^+ decays, which has energy peaking at 1 GeV. Ref [15] has highlighted significant uncertainties in the K^+ production cross sections within this energy range. However, results from the SciBooNE experiment have demonstrated the validity of extrapolating higher energy K^+ data to the 1 GeV region using Feynman scaling [19].

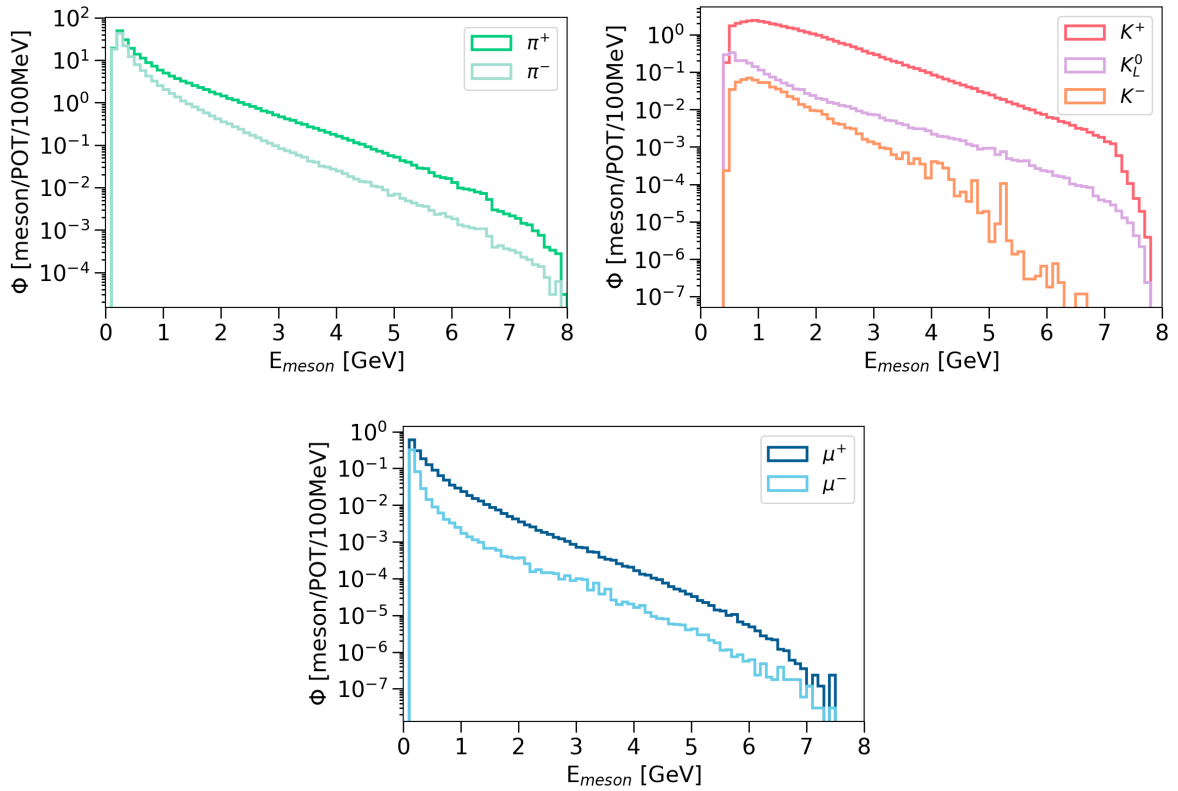


Fig. 4.4 Simulated fluxes of three main contributors to the secondary mesons produced in the BNB as a function of their energies: pions, kaons and muons.

The simulation of the neutrino flux at the front face of SBND is depicted in Fig. 4.5, shown for different flavours of neutrinos. The flux is predominantly composed of ν_μ ($\sim 90\%$), followed by $\bar{\nu}_\mu$ ($\sim 9\%$), while the combination of ν_e and $\bar{\nu}_e$ contributes less than 1%. Fig. 4.6 depicts the parent mesons for each neutrino flavour. Pion production the dominant mechanism for both ν_μ and $\bar{\nu}_\mu$, followed by kaon and muon production. Notably, a peak in

4.2 The Booster Neutrino Beam

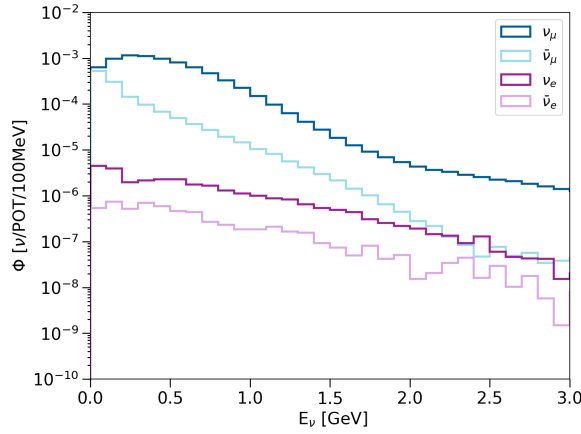


Fig. 4.5 Simulated neutrino fluxes as a function of energy from the BNB at the front face of the SBND detector.

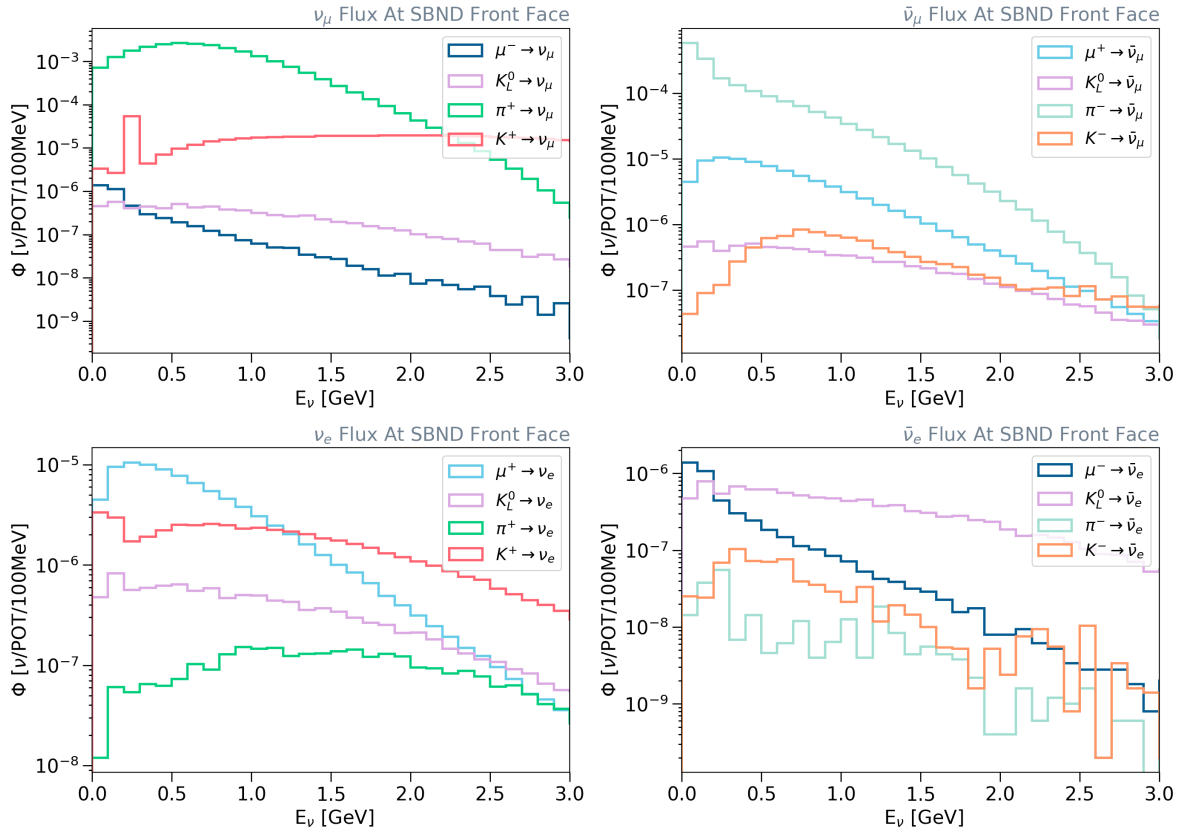


Fig. 4.6 Simulated fluxes for different flavours of neutrino as a function of energy at the front face of SBND, broken down into different types of parent mesons.

the ν_μ flux can be seen at half the mass of the kaon (235.5 MeV) resulting from kaon decay at rest [21]. In the case of ν_e , muons produced from pion decay is the primary source at low energies, while kaon production becomes the dominant mode at higher energies. Finally, $\bar{\nu}_e$ mainly originates from K_L^0 production.

4.3 The Short-Baseline Near Detector

The SBND detector is a LArTPC with an active volume of 112 tons and dimensions of 4 m (x-drift) \times 4 m (y-height) \times 5 m (z-length) [22]. As depicted in Fig. 4.7, the detector consists of two separate TPCs, each with a drift length of 2m, sharing a common Cathode Plane Assembly (CPA) positioned at the centre. A sophisticated Photon Detection System (PDS) is located behind each Anode Plane Assembly (APA) at the edge of the detector. Additionally,

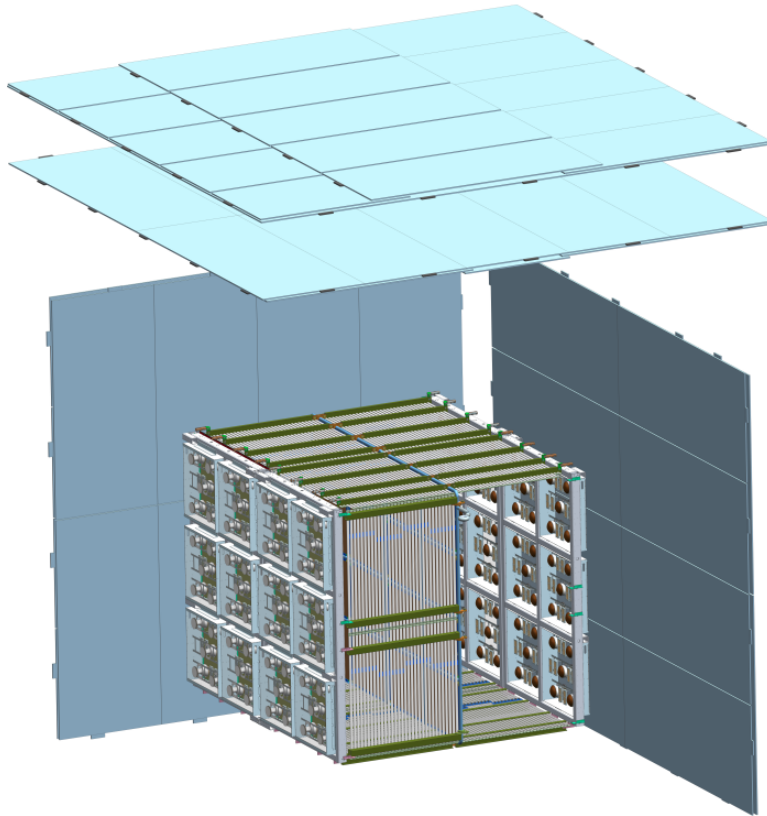


Fig. 4.7 3D modelling of the SBND detector, showing the main LArTPC surrounded by 7 CRT planes. The central CPA divides the detector into two TPCs, each with their own APA and PDS located behind the wire planes.

4.3 The Short-Baseline Near Detector

the PDS incorporates a passive component consisting of TPB-coated reflective foils installed at the CPA. The entire detector is placed inside a membrane cryostat, and then is surrounded by seven planes of Cosmic Ray Tagger (CRT) modules to provide a full solid angle coverage for cosmic rejection.

4.3.1 Time Projection Chamber

The APA planes of the SBND TPC are illustrated in Fig. 4.8. A single APA measures $4\text{ m} \times 2.5\text{ m}$ and comprises a steel frame supporting three wire planes: two induction planes, denoted as U and V, oriented at angles of $\pm 60^\circ$ to the vertical collection plane, denoted as Y. These wire planes U,V and Y are colour-coded as green, blue, and red, respectively. Each wire plane is constructed with $150\text{ }\mu\text{m}$ diameter copper-beryllium wires, with a wire pitch and plane spacing of 3 mm. The wires are tensioned to 7 N to prevent slackening when cooled down to liquid argon temperature at 89 K [23]. To maintain charge transparency for the induction

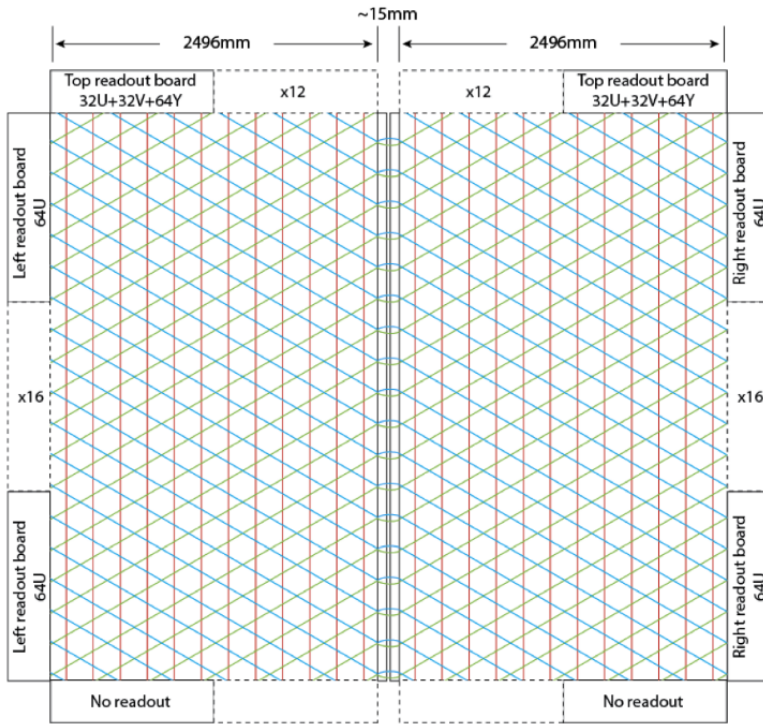
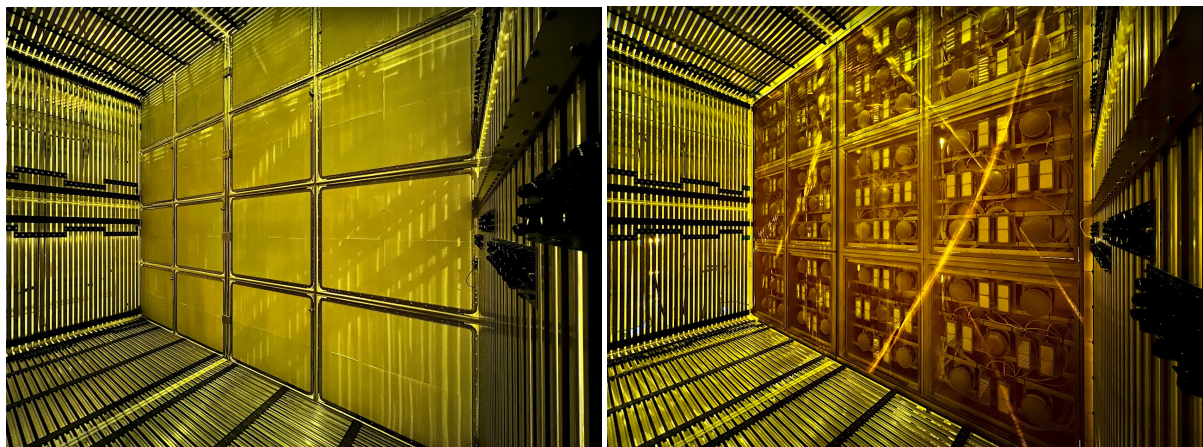


Fig. 4.8 A schematic diagram showing two coupled APAs to form a single APA Plane. The three wire planes U, V, Y are in colour green, blue and red respectively, along side the electronic readout boards. The induction planes of the APAs are coupled together across the 15 mm gap at the centre. Fig. from [22].

planes and collection efficiency for the collection plane, a biased voltage of -200 V, 0 V, and 500 V is applied to planes U, V, and Y, respectively. A pair of coupled APAs together form an APA plane, utilizing jumper cables to bridge the 15 mm gap between the induction planes to form a single electronic channel. In total, each TPC consists of 5,632 wires: 1,664 wires in the collection plane and 1,986 wires in each induction plane.

The CPA plane consists of two steel frames, each containing 8 windows, as illustrated in Fig. 4.9. Each window, measuring 60 cm × 50 cm, houses a fiberglass plate laminated on both sides with non-conductive reflective foils > 99% specular reflection in the visible range and coated with TPB. Furthermore, the plate is covered by a wire mesh, which provides a biased voltage of -100 kV supplied by a high-voltage feedthrough donut from outside the cryostat.

The field cage consists of a sequence of electrodes arranged perpendicular to the drift direction. These electrodes incrementally step up the voltage from -100 kV applied at the CPA to the ground voltage in increments of 3 kV. This gradual voltage increase is implemented to maintain a uniform electric field of 500 V/cm across the drift volume.



(a) View of the CPA

(b) View of the APA

Fig. 4.9 Photographs of the SBND detector during the construction phase at Fermilab. The left photo shows the central CPA housing 16 reflective foils coated with TPB. The right photo shows the APA with the PDS located behind the wires. The field cage can also be seen a series of metal bars surrounding the TPC.

4.3.2 Photon Detection System

The design of the SBND Photon Detection System (PDS), incorporating both active and passive optical components, is the most sophisticated system ever installed in a LArTPC. The active detector integrates two different technologies: (1) a system of 120 Photomultiplier Tubes (PMTs) and (2) a system of 192 X-ARAPUCA devices. The PMTs utilized are cryogenic 8"-diameter Hamamatsu R5912-MOD models [24]. Meanwhile, the X-ARAPUCAs serve as a research and development platform for future experiments, incorporating multiple variations in their components for performance comparison. A summary of the X-ARAPUCA specifications can be found in Ref. []. The TPB-coated reflective foils installed at the CPA is the passive component of the PDS in order to achieve a uniform light yield.

In SBND, the PMT system is the primary light detection system and is utilized to provide trigger conditions. The 120 PMTs are partitioned into two optically-isolated TPC volumes, each with 60 PMTs. Within each TPC, 48 PMTs are TPB-coated, and thus are sensitive to both direct and reflected light components, while the remaining 12 non-coated PMTs detect only reflected light. This ratio of coated to uncoated PMTs (4:1) is chosen to optimize light collection efficiency while maintaining the capability to distinguish between the two light components. Such differentiation improves the reconstruction of scintillation light, which will be discussed in Sec. ??.

For the purpose of installation, the optical detectors are arranged into modular PDS boxes, as depicted on the left side of Fig. 4.10. Each box houses 5 PMTs, 4 coated and 1 uncoated PMT, along with 8 X-ARAPUCA devices, 4 coated and 4 uncoated. These PDS-

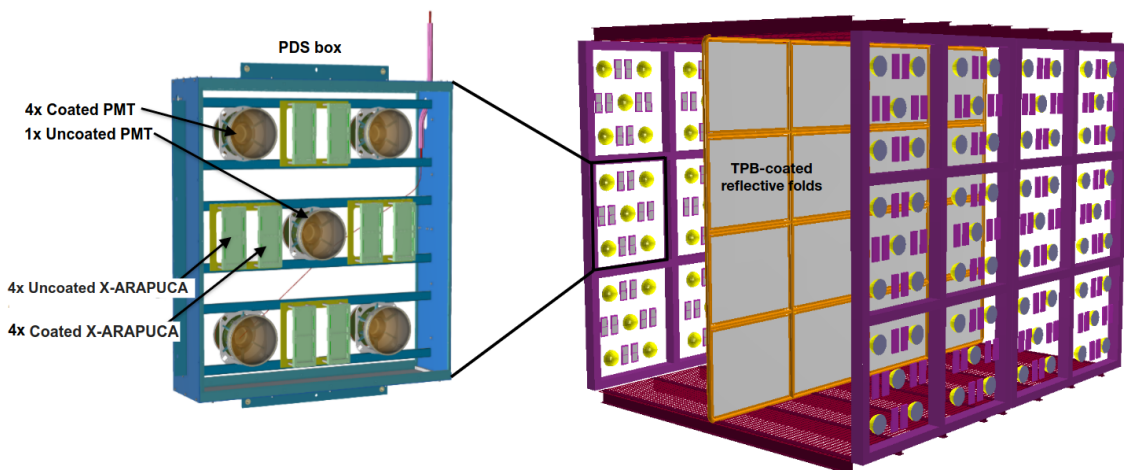


Fig. 4.10 3D modelling of the PMTs and X-ARAPUCAs arrangement in a PDS box (left), together with the PDS boxes installation inside the TPC. Fig. from [].

boxes are installed in a configuration of 4×3 behind each APA plane, resulting in a total of 12 boxes per TPC volume, as illustrated on the right side of Fig. 4.10.

4.3.3 Cosmic Ray Taggers

Since SBND is a surface detector, it utilizes a Cosmic Ray Tagger (CRT) system to effectively reject background from cosmic rays. Each CRT strip consists of a plastic scintillator strip with width of 10.8 cm, connected to a pair of SiPMs via wavelength-shifting optical fibres. These CRT strips are arranged perpendicular to each other to construct a single CRT plane, as depicted in Fig. 4.11, measuring 7.5 m in height and 9 m in width. Coincident hits from perpendicular strips allow for the 2D reconstruction of the hit location, and the number of photons collected for each strip improves the precision of the location tagging. Signals from the SiPMs are amplified, digitized and read out by the Front End Board (FEB) modules with nanosecond timing resolution, which will be detailed in Sec. ??.

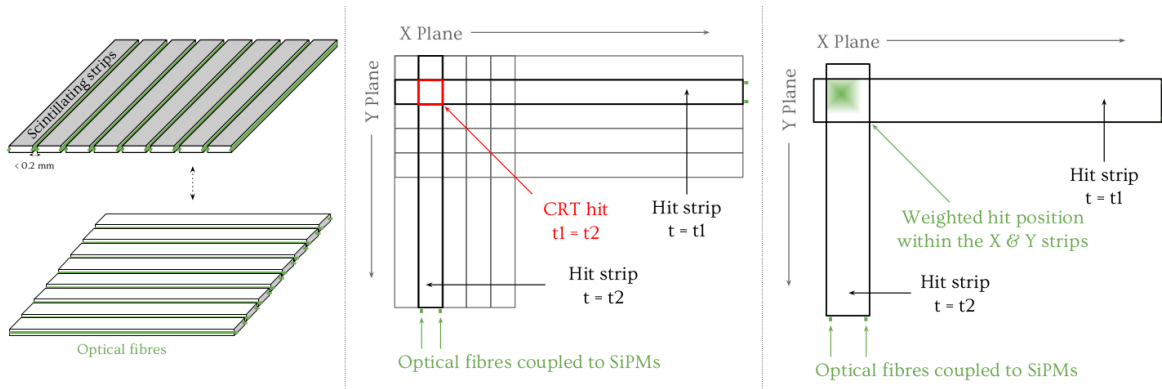


Fig. 4.11 Each CRT plane contains 16 scintillating strips oriented orthogonal to each other (left). Hits coincident in time from perpendicular strips can be used to tag the hit location (middle). The number of photons collected by each hit improves the precision of location tagging (right). Fig. from [25].

As illustrated in Fig. 4.7, SBND is entirely encased by 7 CRT planes, with 1 on each side and 2 positioned atop the detector. This configuration enables a comprehensive strategy for cosmic background rejection utilising both geometrical and high-precision timing information. For instance, tracks identified by the TPC can be matched to CRT hits to identify tracks occurring outside the beam spill window. Additionally, the top 2 planes function as a telescopic array, facilitating the tagging of vertical downward-going cosmic rays.

4.3.4 Trigger

Triggering plays a vital role in the SBND detector, given its close proximity to the BNB and exposure to cosmic rays as a surface detector, resulting in a high rate events. The hardware trigger in SBND is issued by the Penn Trigger Board (PTB), photographed in Fig. 4.12, which receives inputs from the beam system and two detection systems equipped with high timing resolution: the PMTs and CRTs. Notably, SBND marks the first instance of a LArTPC employing the CRT system as part of its triggering mechanism [17]. The PTB then applies programmable trigger logic on the inputs to form triggers. There are three primary types of triggers: (1) the beam trigger for acquiring physics data, (2) the off-beam trigger for estimating cosmic background, and (3) the calibration trigger.

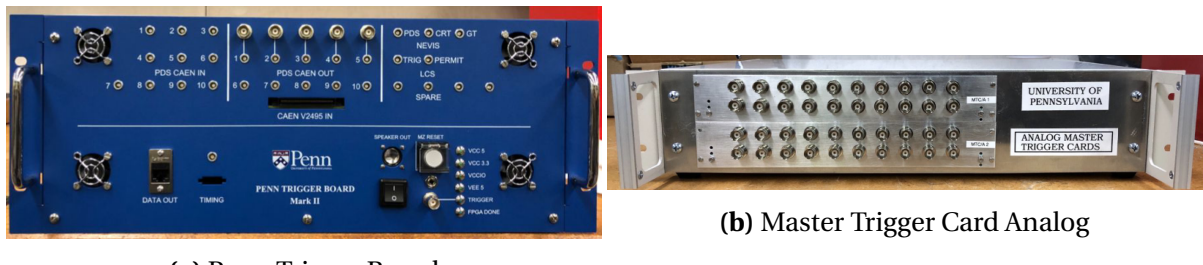


Fig. 4.12 Photographs of the two hardware components in the SBND triggering system.

Diagram in Fig. 4.13 depicts the signal inputs and outputs to and from the PTB to detection subsystems. The beam system informs the PTB about the status of the BNB beam, indicating whether the beam has arrived at the detector hall (shown in green). The PMTs provide information regarding the energy deposited inside the detector (shown in light blue). The number of PMT pairs above a predefined threshold, known as PMT multiplicity, is calculated by the Master Trigger Card Analog (MTC/A) to provide information of the PMT locations (shown in red). The primary beam trigger requires the PMT multiplicity to coincide with the beam window. Conversely, for background estimation purposes, anti-coincidence logic can be applied to estimate the cosmic rate. Meanwhile, the CRT system provides versatile information regarding the topology of cosmic tracks (shown in purple). The calibration trigger utilises the CRTs in coincidence with the PMTs to select cosmic tracks of specific topologies. For example, anode-to-cathode-crossing cosmic tracks can be employed for electron lifetime measurements, which will be explored in Sec. ??.

Once a trigger is formed, the PTB send the signals to subsequent readout subsystems to acquire the event (shown in pink). An event contains two types of trigger signals: a single Event Trigger (ETRIG) and multiple Flash Triggers (FTRIGs). The ETRIG is issued to the TPC

readouts to acquire waveforms from the wire planes. Conversely, FTRIGs are issued to the PDS readouts to capture waveforms from the optical detectors. Further details regarding the data acquisition employing these two types of triggers will be discussed in the following section.

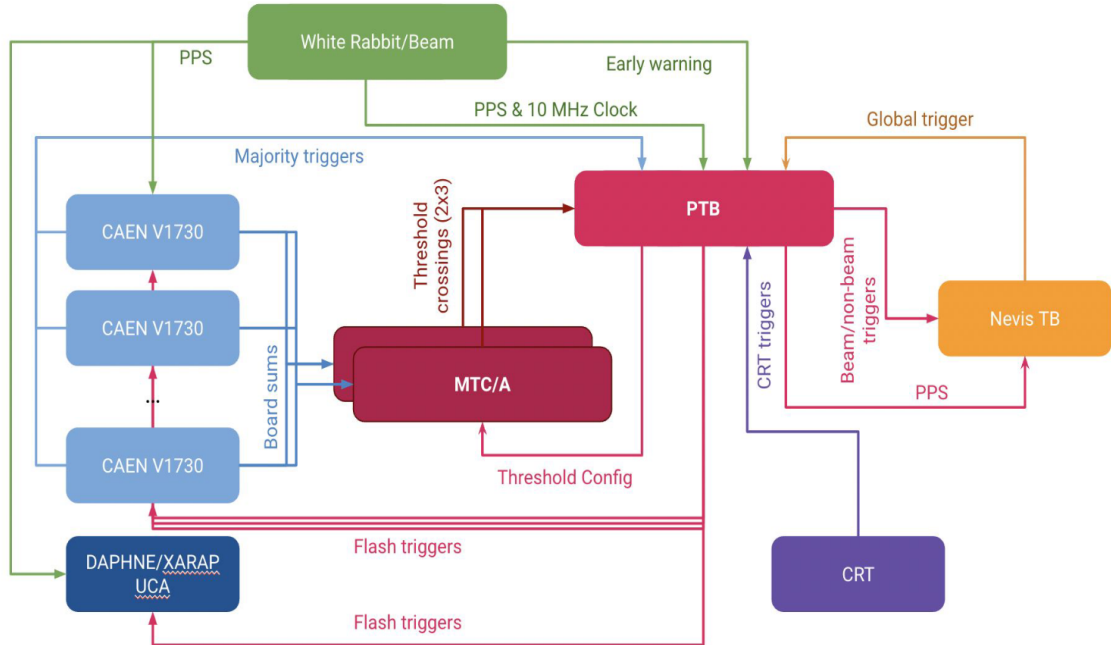


Fig. 4.13 Diagram displaying the flow chart of signals for the hardware triggering system at SBND. Fig. from [1].

4.3.5 Data Acquisition

Data Acquisition (DAQ) is responsible for transporting data from subsystem hardware to event builder machines. During real-time data flow, the DAQ must have the capability for event building by assembling data from each subsystem hardware into a cohesive physics event. Additionally, the DAQ must be able to apply complex software metrics to filter events for various data streams and data monitoring purposes.

At SBND, the DAQ comprises six hardware subsystems illustrated in Fig. 4.1. Among these, four are the detection subsystems: the Time Projection Chamber (TPC), Photomultiplier Tubes (PMTs), X-ARAPUCAs, and Cosmic Ray Taggers (CRTs). Each detection subsystem incorporates specialized hardware components for digitizing and reading out the physical signals. Moreover, two other subsystems are the Penn Trigger Board (PTB) [26] and the SPEC-TDC. The PTB, as a hardware board within the SBND trigger system, is responsible to

4.3 The Short-Baseline Near Detector

provide triggering signals to each detection subsystem independently. The SPEC-TDC is a specialised timing mezzanine module designed specifically for timestamping purposes.

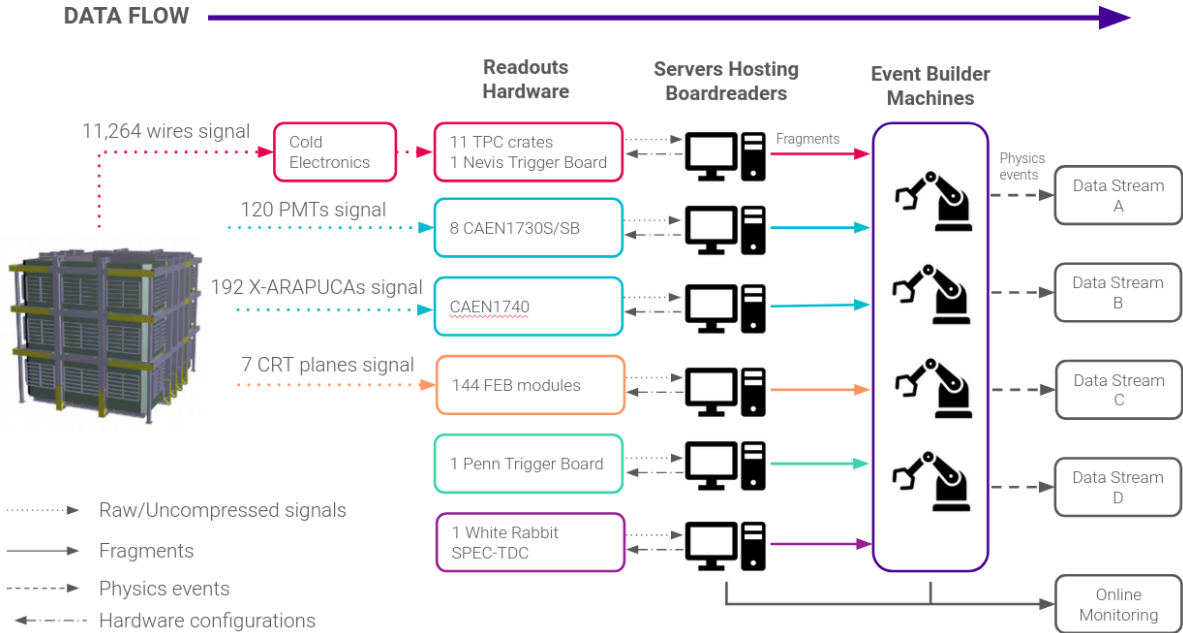


Fig. 4.14 The DAQ system at SBND consists of six subsystems, with four dedicated to detection subsystem readouts for the TPC, CRTs, PMTs and X-ARAPUCAs, while the remaining two facilitate triggering and timing functionalities. Each hardware component is accompanied by a corresponding software boardreader, serving as a communication bridge between the hardware and the event builder machines. The event builders assemble a physics events and send it to different data streams for storage.

The DAQ software framework is provided by the *artdaq Toolkit*, developed by the Real-Time Systems Engineering Department of Fermilab's Scientific Computing Division [27]. The software acts as the backbone of the communication between the hardware components and the event builder machines. The following section provides an overview of the DAQ workflow at SBND as illustrated in Fig. 4.1, describing how signals are acquired from the detection hardware and subsequently digitized by boardreaders and assembled into a physics event.

Within the *artdaq* framework, each discrete hardware readout component has a corresponding software, known as a boardreader, facilitating communication between the readout electronics and the event builder machines. The boardreader can send configurations directly to the hardware in one direction and retrieves data from the hardware in the opposite direction. The data is packaged into a digitized format called a fragment as depicted in Fig. 4.2. The fragment class includes a header containing experiment-specific in-

formation essential for event building, an optional metadata, and a data payload storing the hardware-defined data. A fragment is generated by the boardreader when its corresponding hardware readout receives a trigger. The timestamp of the trigger arrival is encoded in the fragment header, which is known as the fragment timestamp. This timestamp is the crucial value in the event building process.

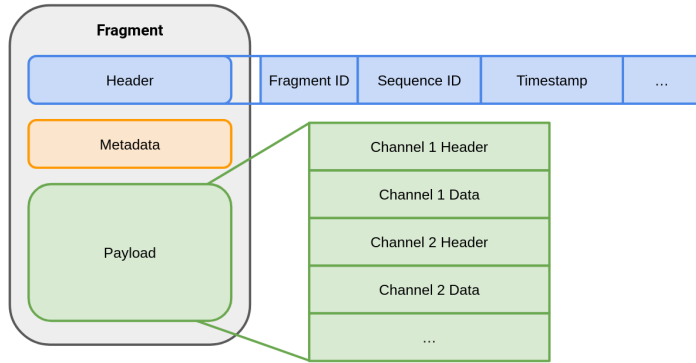


Fig. 4.15 This diagram illustrates the fragment class defined by the *artdaq Toolkit*. The header contains information needed for event building, of which the key information is the fragment timestamp. Optionally, the metadata structure contains hardware configurations. The payload is designated for storing data from the hardware readout, of which the data structure is pre-defined by the hardware.

Once fragments are generated, boardreaders can send them to the event builders in either one of the two configurations: push or pull. When operating in the push configuration, the boardreader actively sends fragments continuously at the rate at which the fragments are generated. The sequence ID of the fragments determines the sequence ID of the built event, ensuring that every fragment is built as a single event. With each fragment sent, the push boardreader also creates a request message, which is multicast to all other boardreaders currently in pull mode. This request message contains the timestamp of the push fragment.

In contrast to the push configuration, the boardreader in the pull configuration stores the fragments in its buffer as the fragments are being generated. These fragments are sent to the event builders only upon receiving a request message. To determine which fragments to send, the boardreader has a configurable parameter called pull window, which specifies a time window relative to the timestamp of the request message. The pull boardreader checks its buffer and selects the fragments with timestamps falling within this defined time window. The selected fragments that meet the timestamp requirement are then dispatched to the event builders. Subsequently, the event builder machines compile this set of fragments, together with one single fragment from the push boardreader that initially generated the

4.3 The Short-Baseline Near Detector

request message, into a single event. The sequence ID of the resulting event is determined by the push fragment.

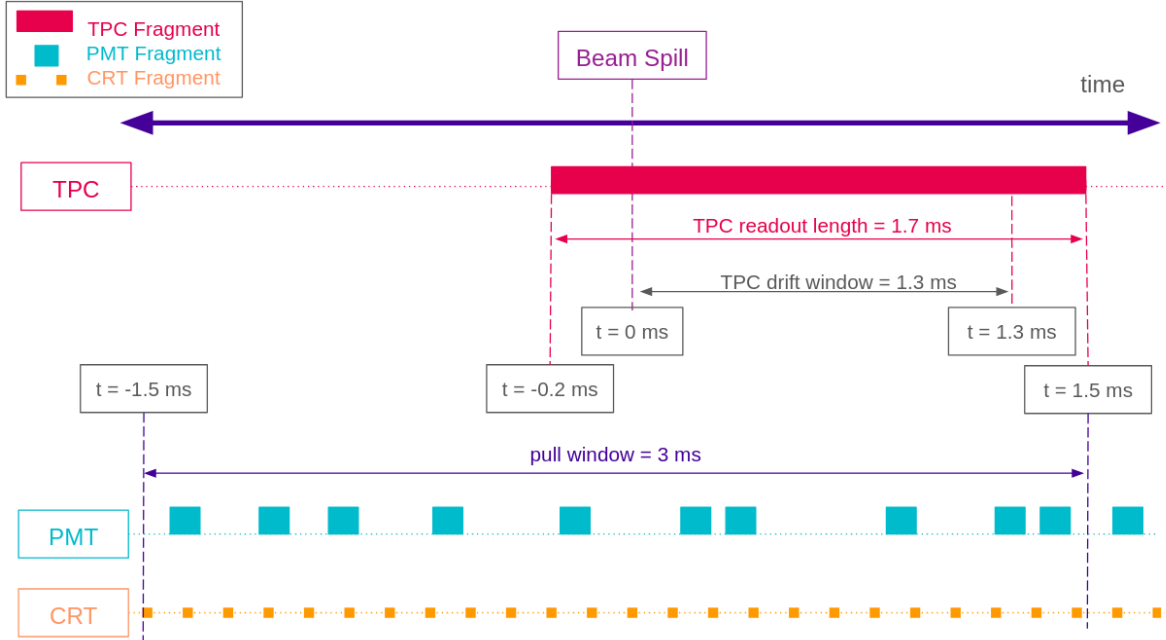


Fig. 4.16 This cartoon depicts a physics event structure at SBND, where the time axis is centred at 0 for when the beam spill begins. The event contains TPC fragments of readout length 1.7 ms to fully cover the drift window of an ionised electron from cathode to anode. The fragments generated by the PMTs and CRTs readouts are included 1.5 ms before and after the beam spill starts. The time asymmetry of the event structure is due to scintillation photon signals are produced and digitised much faster compared to electron signals.

A physics event during a beam spill at SBND is built based on the structure shown in Fig. 4.3, using the fragments from the three detection systems: TPC, PMTs and CRTs.¹ Within this structure, there is only one push boardreader that increments the event sequence ID counter whilst the remaining boardreaders run in pull configuration. The push boardreader is called the Nevis Trigger Board (NTB), which is a component of the hardware complex to readout the TPC data. The NTB sends a single Event trigger to the NTB that coincides with the start of the BNB beam spill if it determines a neutrino event occurs. This generates a TPC fragment with a readout length of 1.7 ms, that fully covers the TPC drift length of 1.3 ms, and includes a padding of 0.2 ms before and after the drift. The Event trigger timestamp is encoded in the NTB fragment header.

¹13th November 2023: The DAQ hardware and software for the X-ARAPUCAs is under development and therefore, not be included in this thesis.

Meanwhile, the boardreaders for the PMTs and CRTs are in pull mode. The PTB sends multiple Flash triggers to the PMTs readouts throughout the beam spill and CRTs readouts are self-triggered independently. The fragment readout lengths from the PMTs and CRTs readouts are much shorter compared to TPC fragments, in the order of μs and ns respectively. The pull window is defined to be 3 ms centred on the timestamp of the NTB fragment, to include PMTs and CRTs fragments generated 1.5 ms before and after the beam spill starts. The event builders then package all the these fragments together to form a physics event.

The event structure has an asymmetry in time due to the physics characteristics of photon signals, detected by the CRTs and PMTs, and electron signals, detected by the TPC wires. Photon signals are much faster than electron signals. A photon produced in CRT scintillator strip takes approximate 5 ns to travel from the far end of the strip until the readouts. A photon produced in the TPC takes maximum 15 ns to arrive at the PMTs from the scintillation location. An ionised electron produced at the same time in the TPC takes 1.3 ms to fully drift from the cathode to the anode. Therefore, scintillation photon signals produced during the beam spill need be digitized and readout much earlier compared to the electron signals.

After the event builder machines complete building a physics event, the resulting event can be filtered and sent to various locations for serving different downstream analysis purposes. This process is commonly referred to as data streaming. The *artdaq Toolkit* provides options to add customisable filtering steps in real-time, such that the event builders can apply complex software metrics based on the fragment contents of an event. Once an event passes the filter, the event builders send it to a location defined by the filter. If an event does not pass the filters, it will be dropped in real-time.

TPC Cold Electronics and DAQ

PDS DAQ

SBND has 120 PMTs as part the Photon Detection System and they are readout by 8 CAENV1730 digitizers [28]. The CAENV1730 digitizer is capable of recording waveforms for 16 channels independently with a sampling rate of 500 MHz. SBND currently uses the model V1730SB which has a deeper buffer to save longer waveform as well as to handle higher data rate. The model also offers better waveform baseline stability against temperature fluctuation. Multiple CAEN digitizers can be synchronised to make up one complex system, such that they all behave as a single digitizer. Thus, the following section evaluates the

4.4 Concluding Remarks

timing precision of CAEN digitizer by characterising the synchronisation across multiple digitizers.

CRT DAQ

The timing resolution of the CRT readout electronics is evaluated in the following section. The CRT detection system consists of 7 CRT planes, and is readout by 144 Front End Board (FEB) modules [29]. A single FEB module a multifunctional board and is capable to serve 32 channels, one channel per Silicon PhotoMultiplier (SiPM). First it can provide a bias voltage which can be adjustable for individual SiPM as well as signal amplification and shaping. Once the signal is shaped, the FEB can apply signal discrimination and self-triggering, such as coincidence for each pair of SiPM and coincidence across multiple FEBs. Once the signal passes the trigger, it is digitised and timestamped with respect to the reference clock. The data is stored in a buffer and readout via Ethernet connection. The following section focuses on the characterisation on the timing resolution of the FEB module.

4.3.6 Data Quality Online Monitoring

The *artdaq Toolkit* also has a built-in process the bridges the event builder machines and online monitoring platforms. Whilst running in real-time, fragments from boardreaders and physics events can be sent to the platforms for different monitoring purposes. SBND currently employs two online platforms that monitors the health of the DAQ: Grafana and Minargon. Grafana, as displayed in Fig. 4.4, provides real-time monitoring of the status of processes being run by boardreaders and event builders. Grafana monitoring also extends to include some status of the respective hardware component for each boardreader. Minargon, as displayed in Fig. 4.5, provides real-time the data quality monitoring. This online monitoring process applies simple reconstruction and event display in order to quantitatively verify the physics characteristics of an event. The author has worked extensively on developing the monitoring processes for the DAQ of the PMTs on both Grafana and Minargon monitoring platforms during her PhD course.

4.4 Concluding Remarks

The Short Baseline Near Detector and The Booster Neutrino Beam

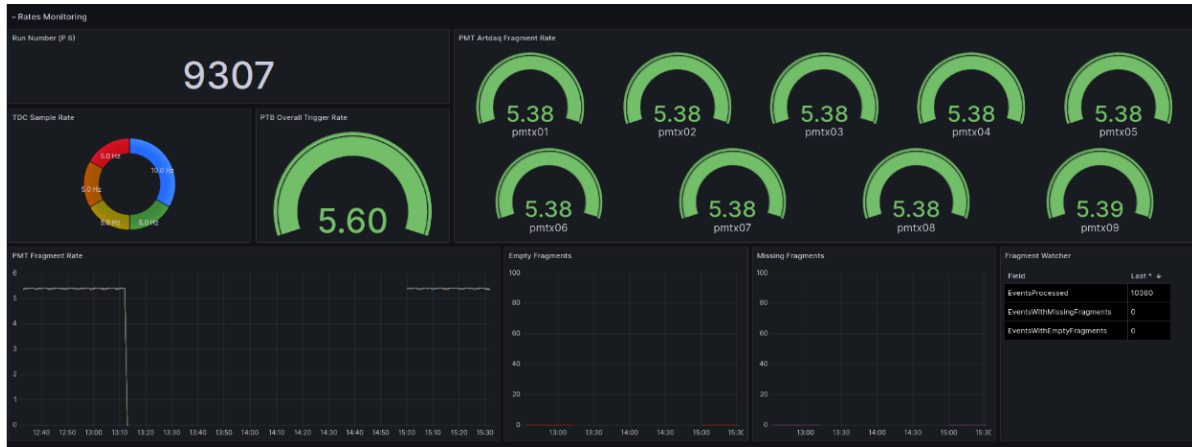


Fig. 4.17 This screenshot displays a section of the Grafana monitoring website for the boardreaders of the PMT DAQ. Some key information to quickly evaluate the status of the PMT boardreaders are shown. For example, the fragment generation rate is expected be consistent with the trigger rate sent by the PTB whilst the empty fragment rate and the missing fragment rate stay flat at zero.

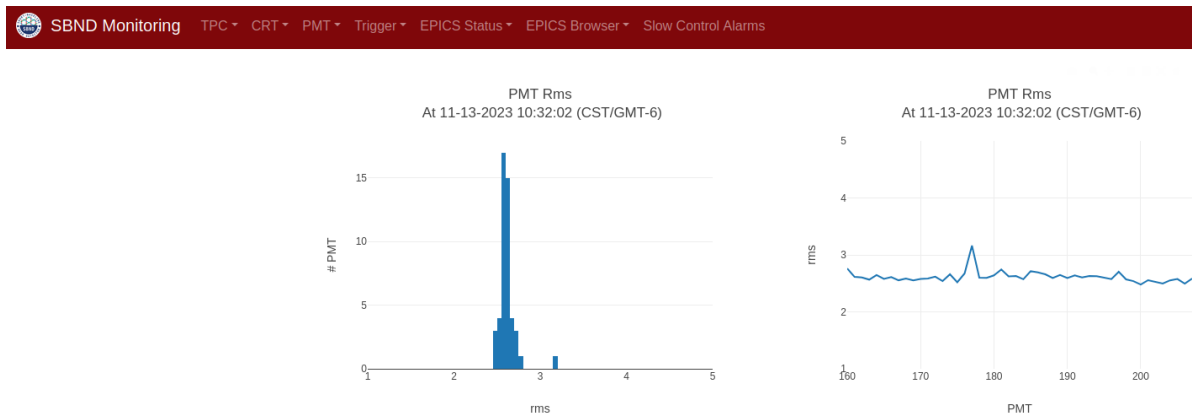


Fig. 4.18 This screenshot displays a section of the Minargon monitoring website to evaluate the quality of data acquired by the PMT DAQ. For example, a metric shown here is the waveform baseline RMS, plotted as a histogram (left) and plotted with respect to the fragment timestamp (right). This metric provides monitoring of the baseline equalisation and stability over time.

References

- [1] P. A. Machado et al., “The Short-Baseline Neutrino Program at Fermilab”, [Annual Review of Nuclear and Particle Science](#) **69**, 363–387 (2019).
- [2] A. Aguilar et al. (LSND Collaboration), “Evidence for neutrino oscillations from the observation of $\bar{\nu}_e$ appearance in a $\bar{\nu}_\mu$ beam”, [Phys. Rev. D](#) **64**, 112007 (2001).
- [3] A. A. Aguilar-Arevalo et al. (MiniBooNE Collaboration), “Significant Excess of Electron-like Events in the MiniBooNE Short-Baseline Neutrino Experiment”, [Phys. Rev. Lett.](#) **121**, 221801 (2018).
- [4] G. Mention et al., “Reactor antineutrino anomaly”, [Phys. Rev. D](#) **83**, 073006 (2011).
- [5] P. Huber, “Determination of antineutrino spectra from nuclear reactors”, [Phys. Rev. C](#) **84**, 024617 (2011).
- [6] Y. J. Ko et al. (NEOS Collaboration), “Sterile Neutrino Search at the NEOS Experiment”, [Phys. Rev. Lett.](#) **118**, 121802 (2017).
- [7] I. Alekseev et al., “Search for sterile neutrinos at the DANSS experiment”, [Physics Letters B](#) **787**, 56–63 (2018).
- [8] W. Hampel et al., “GALLEX solar neutrino observations: results for GALLEX IV”, [Physics Letters B](#) **447**, 127–133 (1999).
- [9] J. N. Abdurashitov et al., “The SAGE and LNGS experiment: Measurement of solar neutrinos at LNGS using gallium from SAGE”, [Astropart. Phys.](#) **25**, 349–354 (2006).
- [10] L. Alvarez-Ruso et al., “NuSTEC White Paper: Status and challenges of neutrino–nucleus scattering”, [Progress in Particle and Nuclear Physics](#) **100**, 1–68 (2018).
- [11] P. Ballett et al., “MeV-scale sterile neutrino decays at the Fermilab Short-Baseline Neutrino program”, [JHEP](#) **04**, 102 (2017).
- [12] V. De Romeri et al., “DUNE-PRISM sensitivity to light dark matter”, [Phys. Rev. D](#) **100**, 095010 (2019).
- [13] E. Bertuzzo et al., “Neutrino masses and mixings dynamically generated by a light dark sector”, [Physics Letters B](#) **791**, 210–214 (2019).
- [14] E. Bertuzzo et al., “Dark Neutrino Portal to Explain MiniBooNE Excess”, [Phys. Rev. Lett.](#) **121**, 241801 (2018).
- [15] A. A. Aguilar-Arevalo et al. (MiniBooNE Collaboration), “Neutrino flux prediction at MiniBooNE”, [Phys. Rev. D](#) **79**, 072002 (2009).
- [16] M. Backfish, *Measuring the Bunch Length of the Booster Neutrino Beamline Beam*, tech. rep. (Fermilab, Nov. 2015).

-
- [17] M. Stancari, “Capabilities of the SBND Trigger System”, in [CPAD Workshop 2022](#) (2022).
 - [18] M. Backfish, *MiniBooNE Resistive Wall Current Monitor*, tech. rep. (Fermilab, Nov. 2015).
 - [19] G. Cheng et al. (SciBooNE Collaboration), “Measurement of K^+ production cross section by 8 GeV protons using high-energy neutrino interactions in the SciBooNE detector”, [Phys. Rev. D 84, 012009 \(2011\)](#).
 - [20] D. W. Schmitz, “A Measurement of Hadron Production Cross Sections for the Simulation of Accelerator Neutrino Beams and a Search for ν_μ to ν_e Sscillations in the δm^2 about equals $1 - eV^2$ Region”, PhD thesis (Columbia U., 2008).
 - [21] J. Spitz, “Sterile neutrino search with kaon decay at rest”, [Phys. Rev. D 85, 093020 \(2012\)](#).
 - [22] R. Acciarri et al. (MicroBooNE, SBND, ICARUS), “A Proposal for a Three Detector Short-Baseline Neutrino Oscillation Program in the Fermilab Booster Neutrino Beam”, (2015).
 - [23] R. Acciarri et al., “Construction of precision wire readout planes for the Short-Baseline Near Detector (SBND)”, [Journal of Instrumentation 15, P06033 \(2020\)](#).
 - [24] *HAMAMATSU Datasheet - R5912*, Accessed: 25-02-2023, https://www.hamamatsu.com/resources/pdf/etd/LARGE_AREA_PMT TPMH1376E.pdf.
 - [25] R. S. Jones, “Muon-neutrino disappearance with multiple liquid argon time projection chambers in the Fermilab Booster neutrino beam”, PhD thesis (The University of Liverpool, 2021).
 - [26] G. V. Stenico, “SBND Trigger System: Status and MTC/A Configuration”, [Physical Sciences Forum 8 \(2023\)](#).
 - [27] K. Biery et al., “Flexible and Scalable Data-Acquisition Using the artdaq Toolkit”, (2018).
 - [28] CAEN SpA, *V1730/VX1730 & V1725/VX1725 User Manual*, 2023.
 - [29] I. Kreslor (SBND Collaboration), *SBND CRT Technical Note*, tech. rep. (2016).